

Global warming can alter shape of the planet, as melting glaciers erode the land

Climate change is causing more than just warmer oceans and erratic weather. According to scientists, it also has the capacity to alter the shape of the planet.

In a five-year study published today in *Nature*, lead author Michele Koppes from the University of British Columbia, compared glaciers in Patagonia and in the Antarctic Peninsula. She and her team found that glaciers in warmer Patagonia moved 100 to 1,000 times faster and caused more erosion than those in Antarctica, as warmer temperatures and melting ice helped lubricate the bed of the glaciers.

Antarctica is warming up, and as it moves to temperatures above zero degrees Celsius, the glaciers are all going to start moving faster. We are already seeing that the ice sheets are starting to move faster and should become more erosive, digging deeper valleys and shedding more sediment into the oceans.

The repercussions of this erosion add to the already complex effects of climate change in the polar regions. Faster moving glaciers deposit more sediment in downstream basins and on the continental shelves, potentially impacting fisheries, dams and access to clean freshwater in mountain communities. The polar continental margins in particular are hotspots of biodiversity, notes Koppes. If you're pumping out that much more sediment into the water, you're changing the aquatic habitat.

The Canadian Arctic, one of the most rapidly warming regions of the world, will feel these effects acutely. With more than four degrees Celsius of warming over the last 50 years, the glaciers are on the brink of a major shift that will see them flowing up to 100 times faster if the climate shifts above zero degrees Celsius.

The findings by Koppes and coauthors also settle a scientific debate about when glaciers have the greatest impact on shaping landscapes and creating relief, suggesting that they do the most erosive work near the end of each cycle of glaciation, rather than at the peak of ice cover. The last major glacial cycles in the Vancouver region ended approximately 12,500 years ago.

Observed latitudinal variations in erosion as a function of glacier dynamics

Michèle Koppes¹, Bernard Hallet², Eric Rignot^{3,4}, Jérémie Mouginot³, Julia Smith Wellner⁵ & Katherine Boldt⁶

Glacial erosion is fundamental to our understanding of the role of Cenozoic-era climate change in the development of topography worldwide, yet the factors that control the rate of erosion by ice remain poorly understood. In many tectonically active mountain ranges, glaciers have been inferred to be highly erosive, and conditions of glaciation are used to explain both the marked relief typical of alpine settings and the limit on mountain heights above the snowline, that is, the glacial buzzsaw¹. In other high-latitude regions, glacial erosion is presumed to be minimal, where a mantle of cold ice effectively protects landscapes from erosion^{2–4}. Glacial erosion rates are expected to increase with decreasing latitude, owing to the climatic control on basal temperature and the production of meltwater, which promotes glacial sliding, erosion and sediment transfer. This relationship between climate, glacier dynamics and erosion rate is the focus of recent numerical modelling^{5–8}, yet it is qualitative and lacks an empirical database. Here we present a comprehensive data set that permits explicit examination of the factors controlling glacier erosion across climatic regimes. We report contemporary ice fluxes, sliding speeds and erosion rates inferred from sediment yields from 15 outlet glaciers spanning 19 degrees of latitude from Patagonia to the Antarctic Peninsula. Although this broad region has a relatively uniform tectonic and geologic history, the thermal regimes of its glaciers range from temperate to polar. We find that basin-averaged erosion rates vary by three orders of magnitude over this latitudinal transect. Our findings imply that climate and the glacier thermal regime control erosion rates more than do extent of ice cover, ice flux or sliding speeds.

Our ability to assess how glacial erosion shapes mountain ranges and reflects climate or tectonic variability is limited by a dearth of information about what controls the rate of glacial erosion, today and in the past. Maximum erosion rates can surpass those of fluvial erosion by up to an order of magnitude^{9,10}, but the few available data sets indicative of rapid glacial erosion are predominantly from massive, fast-moving, temperate tidewater glaciers^{9–11}. In polar regions and many high-altitude alpine settings, glacial erosion is markedly slower^{12,13}. The available data report a wide range of erosion rates from individual ice masses over varying timescales^{9,10,14}, but the cause of this wide range has not been addressed, primarily because of the lack of substantive complementary glaciological data on the ice masses responsible for the erosion.

Recent numerical models have focused on processes that produce glacial landscapes^{5–8,15}. Central to these models is a simple index that relates erosion rate to ice dynamics. Most models assume that erosion rates are proportional to the sliding velocity at the bed^{5–8,15} or the integrated ice discharge¹⁶, and that they reach a peak at the equilibrium-line altitude (ELA). Theory strongly ties the rate of glacial erosion by quarrying and abrasion to the rate of sliding and the effective pressure at the bed, which is controlled by climate through the glacial

thermal regime, ice flux and the amount of meltwater produced^{17,18}. The large meltwater discharge typical of temperate glacial systems evacuates large amounts of debris from under the ice, resulting in massive sediment accumulation at the terminus^{19,20}. In colder climates, glacial erosion is expected to decrease progressively as surface melting decreases, because little or no water reaches the bed to facilitate glacier sliding and flush out any sediment generated from erosion^{21,22}.

Although treatments of glacier dynamics in numerical models have a firm theoretical basis and have become increasingly sophisticated^{5,6}, the parameters that relate erosion to basal sliding remain poorly constrained^{6,7,18}. Most models use a bedrock ‘erosion rule’ of the form $E = K_g u_s^n$, where u_s is the glacier sliding speed, K_g is a constant representing bedrock erosion susceptibility (varying between 10^{-4} and 10^{-6}), and n is a constant that is normally assumed to be one^{5–8,15}. In most cases, the two constants are based on a single empirical study in which both the sediment yield and ice motion were measured at Variegated Glacier, Alaska²³ over a period of a few years that included a major glacier surge. The data we present clearly suggest that the scaling between erosion and sliding rates is strongly affected by the glacier thermal regime.

In an effort to fill this data gap and provide a quantitative test of long-held assumptions, we examine explicitly the factors controlling modern glacier erosion rates across a wide range of climatic regimes. We chose 15 tidewater-outlet glaciers extending from northern Patagonia to the western Antarctic Peninsula (Fig. 1), an area that spans almost 20° of latitude and whose mean annual air temperature varies by 14 °C. This area is an ideal natural laboratory for our purposes: it covers a broad region with a relatively uniform recent tectonic history and bedrock lithologies; it contains a climatically diverse range of glacier thermal regimes that vary from temperate to polar and a transect of glaciers with similar catchment hypsometries; and it is a region where the fjords constitute accessible, natural sediment traps for the products of erosion from the watersheds over the past century. To our knowledge, this is the only transect combining quantitative measurements of both glacier dynamics and erosion rates assembled so far.

Prior studies of sediment accumulation in the region have documented a substantial decrease in sedimentation in the fjords from north to south and west to east^{24–26}, which has been inferred to reflect climate-driven differences in glacier dynamics and meltwater. Here we take a more quantitative approach and focus on the past 50–100 years, for which considerable data exist on both the glaciers and sediment yields. For each glacier catchment, we estimate the contemporary sediment yield using two complementary approaches, as required by the large range of sedimentation rates and the time span of interest. First, we calculate the sediment volume in recently deglaciated fjords from acoustic reflection profiles, repeat bathymetry and the history of glacial retreat¹¹ (for all but one of the glaciers in Patagonia). Second, we calculate the product of the accumulation rate using published ²¹⁰Pb

¹Department of Geography, 1984 West Mall, University of British Columbia, Vancouver, British Columbia V6T 1Z2, Canada. ²Department of Earth and Space Sciences and Quaternary Research Center, Box 351310, University of Washington, Seattle, Washington 98195-1310, USA. ³Department of Earth System Science, University of California, Irvine, California 92617, USA. ⁴NASA Jet Propulsion Laboratory, Pasadena, California 91109, USA. ⁵Department of Earth and Atmospheric Sciences, University of Houston, Houston, Texas 77204, USA. ⁶School of Oceanography, Box 357940, University of Washington, Seattle, Washington 98195-7940, USA.

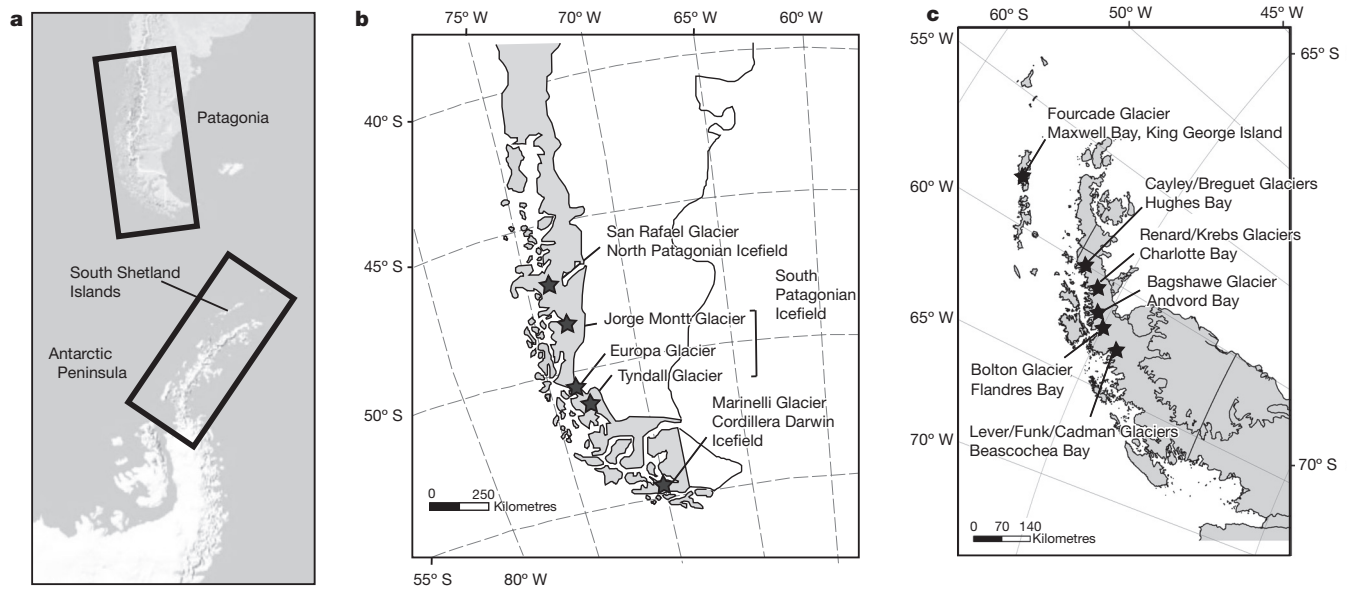


Figure 1 | Location map of study area, from northern Patagonia to central Antarctic Peninsula. **a**, Entire latitudinal transect from 46° S to 66° S. **b**, **c**, Location of glaciers and adjacent fjords in Chilean Patagonia (**b**), and the South Shetland Islands and the Antarctic Peninsula (**c**).

analyses of sediment cores^{20,27} and the spatial extent of the fjord depocentres (zones of subaqueous sediment deposition) measured from multibeam swath bathymetry. We determine the basin-averaged erosion rates over the past 50–100 years on the basis of the ratio of sediment yield to the area of the glacier-drainage basin. We then compare the erosion rates to simple indices of the contemporary dynamics of the glaciers that produced and delivered the sediment, that is, the ice flux and basal sliding velocity at the ELA. This study highlights the influence of both climate and glacier dynamics on the broad spatial pattern of contemporary glacial erosion, and leads to broader insights into the temporal variation in erosion rates seen in glaciated orogens. We take a ‘trading space for time’ approach by comparing glacier systems with similar basin characteristics but differing climatic regimes to quantify the impact of climate change on erosion rates over glacial–interglacial cycles.

The climatic conditions from the Patagonian Andes to the western Antarctic Peninsula support ice masses on mountains that rise up to 3,500 m above sea level, with glaciers terminating at sea level. In Patagonia, the ELA ranges from 700 m to 1,300 m above sea level²⁸; in the western Antarctic Peninsula, on the basis of the late summer snowlines, the ELA is just above the calving fronts²⁴. All of our study sites are north of 70° S in the ‘wet snow’ zone, where glaciers experience occasional to frequent surface melting in late summer²⁹, which suggests the potential for meltwater to access the glacier bed and for sliding and active erosion at the ice–bed interface.

On the timescale of the last 50–100 years, basin-averaged bedrock erosion rates along our 19° N–S transect vary by three orders of magnitude, largely as a function of temperature (Fig. 2). For each glacier, the erosion rate and corresponding glaciological information are compiled in Extended Data Table 1. Some of the most rapidly eroding contemporary glacial systems worldwide^{10,11} are found at the northern end of our transect. Basin-wide erosion rates range from 12 mm yr⁻¹ at San Rafael Glacier in the north to 0.01 mm yr⁻¹ at Funk Glacier in the polar south. As seen in Fig. 2a and b, the erosion rates show a significant correlation with latitude ($r^2 = 0.75$, $n = 13$) and mean annual temperature ($r^2 = 0.81$, $n = 13$).

Along our transect, erosion rates also increase nonlinearly with both the sliding speed and the ice flux through the ELA (Fig. 2c, d), suggesting a weak power-law relationship with both ice discharge and basal speed ($r^2 = 0.21$ and $r^2 = 0.39$, respectively). This nonlinear

relationship is in accord with theories of glacial erosion, where an increase in basal ice velocities is expected to increase both quarrying rates and the flux of debris available to abrade the bed^{17,18}. The two outliers in this general trend are Tyndall Glacier and Fourcade Glacier; excluding these two systems, the correlation between erosion and sliding improves substantially ($r^2 = 0.62$; Extended Data Fig. 1).

We caution that several sources of uncertainty in our measurements of both erosion rate and ice motion may confound simple relationships between the two parameters. For instance, the sediment yield and inferred erosion rate for Europa Glacier are abnormally low for its size, speed and climate, which probably reflects both reduced erosion and the trapping of sediments in a deep subglacial basin. Europa is the only Patagonian glacier in our data set that has not undergone substantial thinning and terminus retreat in the past 50 years³⁰, and hence we are not yet seeing the increase in sediment yield that has been observed to accompany glacial retreat^{10,11}. Moreover, at Europa Glacier, surface speeds decrease sharply with distance from the terminus and remain low 8–15 km upglacier of the terminus (see Extended Data Figs 2 and 3). Mass (ice) conservation suggests that this decrease in surface speed, combined with low surface slopes, reflects an abrupt increase in ice thickness and an extensive subglacial overdeepening. Shallow slopes and overdeepenings with steep outlets favour the storage of sediment at the bed, both reducing sediment delivery to the ice front and protecting the bed from further erosion. Moreover, there is no obvious submarine sill or moraine in the outer fjord to trap all the products of glacial erosion. Topographic controls on subglacial and proglacial sediment storage and evacuation are sources of uncertainty in all of our glacier–fjord systems, but are most pronounced for this catchment; see Methods for further discussion of the uncertainties with these estimates.

Notwithstanding the complexities inherent in our observational data, the modern erosion rates for the western Antarctic Peninsula (0.01 mm yr⁻¹ to <0.1 mm yr⁻¹) are two orders of magnitude lower than the rates for the Patagonian glaciers (1 mm yr⁻¹ to >10 mm yr⁻¹). This difference exists despite overlapping ice fluxes and sliding speeds. Within the western Antarctic Peninsula, our erosion rates are within the range reported previously in polar fjords in the Arctic^{12,13,23}. The erosion rates in this region also tend to increase with increasing glacier size and speed. The over 100-fold lower erosion rates in the Antarctic Peninsula suggest both less vigorous glacial erosion and less delivery of sediment generated at the bed to the ice front and

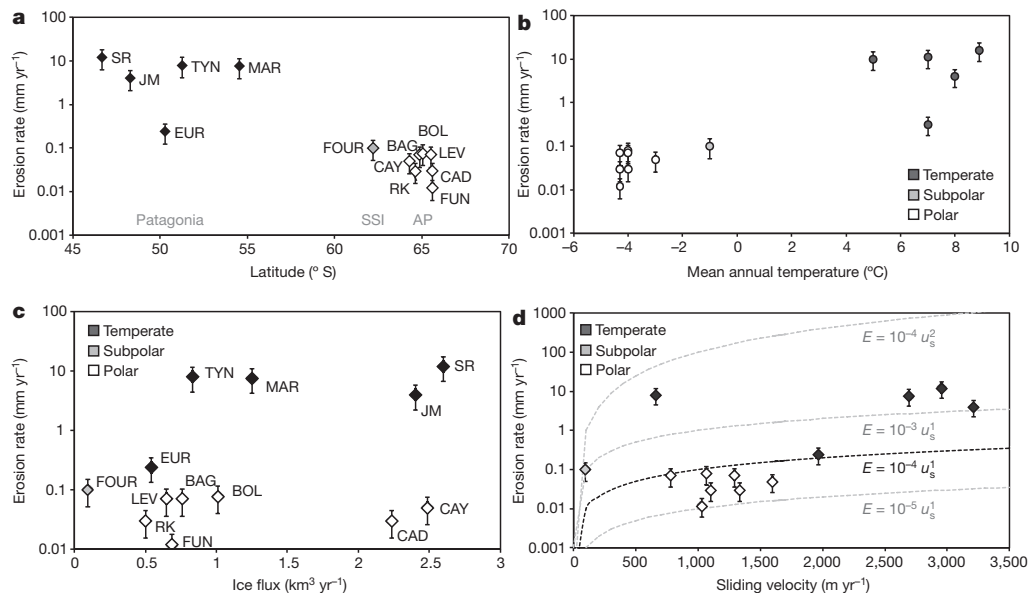


Figure 2 | Erosion rate as a function of latitude, climate and dynamics of 13 outlet glaciers. **a–d**, Erosion rate versus latitude (**a**; SSI, South Shetland Islands; AP, Antarctic Peninsula), mean annual air temperature, estimated from ref. 32 (**b**), ice flux (**c**) and basal sliding speed, with dashed lines representing commonly used forms of the ‘erosion rule’ (as labelled, the black

dashed line corresponds to the most commonly used form) in landscape-evolution models^{5–8,15,18} (**d**). Error bars denote $\pm 50\%$ uncertainty in determining sediment volume and basin-averaged bedrock erosion rate. For definitions of glacier acronyms, see Extended Data Table 1.

the fjord beyond by the subglacial hydrologic system. Further work is needed to better resolve the effect of such changes in sediment evacuation rates on the sediment yields observed over these timescales, which could confound inferred erosion rates. As suggested above, this is most probably the case for Europa Glacier.

For glaciers of similar ice flux or sliding speed across the thermal spectrum, erosion rates for polar glaciers are lower by over two orders of magnitude than for temperate glaciers with similar ice discharges (Fig. 2c). We suggest that this difference for glaciers of similar size and motion is primarily related to the abundance of meltwater accessing the bed. This is in accord with the concept that frequent and rapid fluctuations in the basal water pressure, which are more likely in regions where meltwater production is seasonal, promote both subglacial quarrying rates and efficient sediment evacuation by subglacial rivers^{17,18}. Patagonia is one such region, where the relatively warm climate and heavy precipitation augment both surface and internal melting, thereby increasing the supply of water to the glacier bed, which promotes sliding, erosion, and sediment production and evacuation⁵. For example, annual surface melt rates approach 2 m and 6 m water equivalent at Marinelli and San Rafael glaciers, respectively. In contrast, in the western Antarctic Peninsula, sub-freezing temperatures for much of the year, melt rates of approximately 0.1 m water equivalent per year and ice thicknesses of >300 m suggest that little, if any, surface melt generated can infiltrate the glaciers without refreezing³¹.

From temperate to polar settings, modern erosion rates measured from systems of similar catchment size, ice flux, tectonic history and bedrock lithology slow by over two orders of magnitude (Fig. 2). A similar decrease, which we see in space from temperate to polar settings, is widely recognized in time from data representing recent to long-term (million-year) erosion rates derived from sediment traps, cosmogenic dating and low-temperature thermochronometers from the same glaciated catchment^{10,14}. Because all glaciers worldwide have experienced generally colder-than-current climatic conditions throughout the late Quaternary period, the 100-fold decrease in long-term relative to modern erosion rates, particularly for currently temperate glaciers in Patagonia^{2,14}, may reflect (in part) the temporal averaging of warm- and cold-based conditions over the lifecycle of

these glaciers. On the basis of our ‘trading space for time’ analysis, and the 100-fold difference in erosion rates captured along our latitudinal transect, we expect a substantial acceleration in erosion rates and in sediment delivery from the glaciers of the Antarctic Peninsula region as they transition to more temperate conditions in the coming century²¹.

Recent numerical modelling efforts have successfully replicated glacial landscapes when erosion rates are assumed to scale linearly with basal sliding speed^{5–8,15,16}. Our results augment these models by providing field calibration of rates of erosion and sliding, and highlight the seldom-recognized importance of the effect of surface temperature on the erosion rate. Our findings indicate that erosion rates from glaciers under a broad range of thermal regimes are highly variable. We propose that climatic variation, more than ice dynamics, controls the temporal and spatial variability in erosion rates, and that a mean annual temperature above $0\text{--}5^\circ\text{C}$ (implying ample supplies of subglacial meltwater) constitutes a threshold condition for fast glacial erosion. Our findings reinforce the link between erosional processes and global climate, and help explain the role of climate change in the development of topography over glacial–interglacial timescales.

Online Content Methods, along with any additional Extended Data display items and Source Data, are available in the online version of the paper; references unique to these sections appear only in the online paper.

Received 8 June 2014; accepted 27 July 2015.

- Egholm, D. L., Nielsen, S. B., Pedersen, V. K. & Lesemann, J.-E. Glacial effects limiting mountain height. *Nature* **460**, 884–887 (2009).
- Thomson, S. N. *et al.* Glaciation as a destructive and constructive control on mountain building. *Nature* **467**, 313–317 (2010).
- Koons, P. O. The topographic evolution of collisional mountain belts: a numerical look at the Southern Alps, New Zealand. *Am. J. Sci.* **289**, 1041–1069 (1989).
- Stroeven, A. P., Fabel, D., Hatterstrand, C. & Harbor, J. A relict landscape in the centre of the Fennoscandian glaciation: cosmogenic radionuclide evidence of tors preserved through multiple glacial cycles. *Geomorphology* **44**, 145–154 (2002).
- Egholm, D. L., Pedersen, V. K., Knudsen, M. F. & Larsen, N. K. Coupling the flow of ice, water, and sediment in a glacial landscape evolution model. *Geomorphology* **141–142**, 47–66 (2012).
- Herman, F., Beaud, F., Champagnac, J.-D., Lemieux, J.-M. & Sternai, P. Glacial hydrology and erosion patterns: a mechanism for carving glacial valleys. *Earth Planet. Sci. Lett.* **310**, 498–508 (2011).
- Yanites, B. & Ehlers, T. A. Global climate and tectonic controls on the denudation of glaciated mountains. *Earth Planet. Sci. Lett.* **325–326**, 63–75 (2012).

8. Tomkin, J. H. Numerically simulating alpine landscapes: the geomorphic consequences of incorporating glacial erosion in surface process models. *Geomorphology* **103**, 180–188 (2009).
9. Hallet, B., Hunter, L. & Bogen, J. Rates of erosion and sediment evacuation by glaciers: a review of field data and their implications. *Global Planet. Change* **12**, 213–235 (1996).
10. Koppes, M. & Montgomery, D. The relative efficacy of fluvial and glacial erosion over modern to orogenic timescales. *Nature Geosci.* **2**, 644–647 (2009).
11. Koppes, M., Hallet, B. & Anderson, J. Synchronous acceleration of ice loss and glacier erosion, Marinelli Glacier, Tierra del Fuego. *J. Glaciol.* **55**, 207–220 (2009).
12. Szczuciński, W., Zajączkowski, M. & Scholten, J. Sediment accumulation rates in subpolar fjords—impact of post-Little Ice Age glaciers retreat, Billefjorden, Svalbard. *Estuar. Coast. Shelf Sci.* **85**, 345–356 (2009).
13. Cowton, T., Nienow, P., Bartholomew, I., Sole, A. & Mair, D. Rapid erosion beneath the Greenland Ice Sheet. *Geology* **40**, 343–346 (2012).
14. Fernandez, R. A., Anderson, J. B., Wellner, J. S. & Hallet, B. Timescale dependence of glacial erosion rates: a case study of Marinelli Glacier, Cordillera Darwin, southern Patagonia. *J. Geophys. Res.* **116**, F01020 (2011).
15. MacGregor, K. R., Anderson, R. S. & Waddington, E. D. Numerical modeling of glacial erosion and headwall processes in alpine valleys. *Geomorphology* **103**, 189–204 (2009).
16. Kessler, M. A., Anderson, R. S. & Briner, J. P. Fjord insertion into continental margins driven by topographic steering of ice. *Nature Geosci.* **1**, 365–369 (2008).
17. Hallet, B. Glacial quarrying: a simple theoretical model. *Ann. Glaciol.* **22**, 1–8 (1996).
18. Iverson, N. R. A theory of glacial quarrying for landscape evolution models. *Geology* **40**, 679–682 (2012).
19. Cowan, E. A. *et al.* Fjords as temporary sediment traps: history of glacial erosion and deposition in Muir Inlet, Glacier Bay National Park, southeastern Alaska. *Geol. Soc. Am. Bull.* **122**, 1067–1080 (2010).
20. Boldt, K. V. *et al.* Modern rates of glacial sediment accumulation along a 15° S–N transect in fjords from the Antarctic Peninsula to southern Chile. *J. Geophys. Res.* **118**, 2072–2088 (2013).
21. Cuffey, K. M., Conway, H., Hallet, B., Gades, A. & Raymond, C. F. Interfacial water in polar glaciers and glacier sliding at -17°C . *Geophys. Res. Lett.* **26**, 751–754 (1999).
22. Hooke, R. & Elverhøi, A. Sediment flux from a fjord during glacial periods, Isfjorden, Spitsbergen. *Global Planet. Change* **12**, 237–249 (1996).
23. Humphrey, N. F. & Raymond, C. F. Hydrology, erosion and sediment production in a surging glacier: Variegated Glacier, Alaska, 1982–83. *J. Glaciol.* **40**, 539–552 (1994).
24. Griffith, T. W. & Anderson, J. B. Climatic control of sedimentation in bays and fjords of the northern Antarctic Peninsula. *Mar. Geol.* **85**, 181–204 (1989).
25. DaSilva, J. L., Anderson, J. B. & Stravers, J. Seismic facies changes along a nearly continuous 24° latitudinal transect: the fjords of Chile and the northern Antarctic Peninsula. *Mar. Geol.* **143**, 103–123 (1997).
26. Hebbeln, D., Lamy, F., Mohtadi, M. & Echtler, H. Tracing the impact of glacial-interglacial climate variability on erosion of the southern Andes. *Geology* **35**, 131–134 (2007).
27. Domack, E. W. & McClennen, C. E. Accumulation of glacial marine sediments in fjords of the Antarctic Peninsula and their use as late Holocene paleoenvironmental indicators. *Antarct. Res. Ser.* **70**, 135–154 (1996).
28. Rignot, E., Rivera, A. & Casassa, G. Contribution of the Patagonia Icefields of South America to sea level rise. *Science* **302**, 434–437 (2003).
29. Rau, F. & Braun, M. The regional distribution of the dry-snow zone on the Antarctic Peninsula north of 70° S. *Ann. Glaciol.* **34**, 95–100 (2002).
30. Sukakibara, D. & Sugiyama, S. Ice-front variations and speed changes of calving glaciers in the Southern Patagonia Icefield from 1984–2011. *J. Geophys. Res.* **119**, 2541–2554 (2014).
31. Lenaerts, J. T. M., van den Broeke, M. R., van den Berg, W. J., van Meijgaard, E. & Kuipers Munneke, P. A new, high-resolution surface mass balance map of Antarctica (1979–2010) based on regional atmospheric climate modeling. *Geophys. Res. Lett.* **39**, L04501 (2012).
32. Morris, E. M. & Vaughan, D. G. in *Antarctic Peninsula Climate Variability* (eds Domack, E. *et al.*) Vol. 79 of *Antarctic Research Series* 61–68. (American Geophysical Union, 2003).

Acknowledgements This research was funded by the US National Science Foundation (OPP 0338371). We thank the crews of the ice breaker RV *Nathaniel B. Palmer* and the MV *Petrel IV*, members of Waters of Patagonia, support staff from Raytheon Polar Services, and collaborators from the Centro de Estudios Científicos in Valdivia, Chile, the University of Washington, Rice University and the University of Houston for assisting in deployments, sampling and analysis of the sediment cores, bathymetric data, ice front geometries and acoustic reflection profiles collected during the cruises. We particularly thank J. Anderson, A. Rivera, M. Jaffrey, J. Evans and T. Verzone for help and logistical support in the field; R. Sylwester for his contribution to the collection of acoustic reflection profiles in Chile; C. Nittrouer, B. Forrest, C. Landowski, J. Berquist and T. Drexler for processing and analysing the sediment cores; T. Pratt for processing of acoustic profiles in Jorge Montt; J. Anderson and R. Fernandez for supporting data and discussions; C. Brookfield for editing and insight; R. Jaña at INACH for provision of Landsat imagery of the Antarctic Peninsula; and M. Jaffrey, J. Newton and A. Winter-Billington for help with statistical analyses.

Author Contributions M.K., B.H. and J.S.W., together with J. Anderson, designed the study. M.K. conducted all analyses of glaciological and erosion-rate data, and prepared the manuscript. E.R. and J.M. contributed the ice-velocity measurements. K.B. contributed the accumulation-rate results, and provided new data for Jorge Montt Glacier. J.S.W. and K.B. analysed the bathymetric data, acoustic profiles and sediment cores in the Antarctic Peninsula fjords. All authors contributed to discussions and interpretations.

Author Information Reprints and permissions information is available at www.nature.com/reprints. The authors declare no competing financial interests. Readers are welcome to comment on the online version of the paper. Correspondence and requests for materials should be addressed to M.K. (koppes@geog.ubc.ca).

METHODS

Geologic setting. Southern Chile and the Antarctic Peninsula share the tectonic and geologic history of the Andean orogen, the product of a long history of ocean-continent collision and ridge subduction since the mid-Palaeozoic era³⁵. From the Late Palaeozoic to the Tertiary period, the southern Andes and the northern Antarctic Peninsula have been in a state of tectonic compression and experiencing coeval island-arc marginal basin evolution, giving rise to a thick sequence of fore-arc sedimentary basin deposits intruded by calc-alkaline plutons³⁴. Since the Neogene period, subduction of the Nazca–Antarctic and Phoenix–Antarctic spreading ridges has produced the Patagonian and Antarctic slab windows, giving rise to the interruption of normal calc-alkaline arc volcanism, the eruption of plateau basalts in southern South America and the Antarctic Peninsula³⁴, and the broad uplift of both continents through a dynamic topographic response³⁵. These slab windows persist today, producing persistent mantle upflow, broad regional uplift and basaltic magmatism that overlie the plutons and sedimentary basin deposits³⁴. Thus, relatively resistant metasediments, intrusive granite batholiths, and mafic metavolcanics are the predominant rock types that underlie the icefields from Patagonia to the Antarctic Peninsula, with bed resistances within a relatively narrow range.

Climatic setting. The climate along our transect varies from the warm and wet sector of Patagonia in southern Chile, to a transitional climate in the South Shetland Islands, to the relatively cold and dry western Antarctic Peninsula. The study area spans almost 20° of latitude and has mean annual air temperatures (MAT) that vary by 14 °C, encompassing temperate, subpolar and polar glaciers that range from the lowest-latitude tidewater glacier in the world, San Rafael Glacier (46.6° S, MAT = 9 °C), to Cadman Glacier, Beascochea Bay (65.6° S, MAT = –5 °C). Precipitation rates at sea level range from about 7 m yr^{–1} in southern Patagonia to about 1 m yr^{–1} in the western Antarctic Peninsula.

At the northern end of our transect, westerly winds create a large E–W precipitation gradient along Chile’s southern coast. Near the core of the westerlies at 50° S, the latitude of the South Patagonian Icefield (Fig. 1b), at sea level, the mean annual temperature is approximately 7 °C and precipitation reaches 7 m yr^{–1}. To the north, at the latitude of San Rafael Glacier (46° S), precipitation decreases to about 4 m yr^{–1} and mean annual temperatures at sea level average approximately 9 °C. To the south, in the Cordillera Darwin Icefield (54° S), precipitation rates are closer to 1 m yr^{–1} and mean annual temperatures are 5 °C at sea level. Owing to the relatively warm and wet setting of Chilean Patagonia, all of the ice masses are temperate and have presumably been temperate since the early Holocene³⁶.

The South Shetland Islands lie close to the northern tip of the Antarctic Peninsula (Fig. 1a, c). Land- and marine-terminating ice masses, with a mean thickness of approximately 250 m, cover the islands. The climatic conditions vary between subpolar and temperate, with winter temperatures between –3 °C and –5 °C, and late summer temperatures above freezing³². This area has experienced 3.7 ± 2.1 °C of warming in the last century—the second-fastest warming documented worldwide³⁷. Of the total annual precipitation of about 1.2 m, approximately 0.2 m falls as rain during the summer: it contributes to substantial ablation and adds surface water to the lower reaches of the icefields, where late summer snowlines vary around approximately 150 m above sea level³⁸.

Along the western margin of the Antarctic Peninsula, the climate varies from polar to subpolar and mean temperatures range from about 0 °C in the austral summer to –8 °C to –11 °C in the winter³⁸. Average precipitation at sea level along the western Antarctic Peninsula varies from approximately 0.8 m water equivalent per year at Andvord Bay to approximately 1 m water equivalent per year at Beascochea Bay³⁸, all as snow. The narrow N–S spine of the Antarctic Peninsula, much like in the Patagonian Andes, creates a strong orographic gradient that supports a narrow plateau of ice, with steep, narrow outlet glaciers cascading to the west from the summit plateau and terminating at sea level.

The Antarctic Peninsula is one of the most rapidly warming regions in the world, with an increase in MAT of 3.7 ± 1.6 °C over the past century³². Over the last 50 years, the most rapid warming recorded in Antarctica of 5.7 ± 2.0 °C per century was measured at Faraday Station (65.2° S, 64.3° W), near Beascochea Bay³⁷. The glaciers of the western Antarctic Peninsula are already showing substantial variability in both contemporary ice fluxes and in retreat rates in response to the rapid regional warming^{39–41}. The sediment output (and hence erosion rate) is expected to increase as these glaciers accelerate and as a more robust subglacial hydrologic system flushes out sediment that may have been stored under the glaciers. Hence, we expect further changes in ice dynamics and associated increases in erosion rates as the region continues to warm, particularly as many of the outlet glaciers of the Antarctic Peninsula have already started to accelerate as climatic conditions shift to a more temperate regime³⁷.

Calculating contemporary ice fluxes and sliding speeds. The contemporary ice flux through each glacier system was reconstructed, with the exception of the glaciers mentioned below, by multiplying the cross-sectional area of the ice front

with the depth-averaged velocity near the terminus, based on surface-velocity measurements using synthetic-aperture-radar interferometry (InSAR)^{42–44} (Extended Data Fig. 2)

For the five Patagonian glaciers, we use previously published estimates of the surface speed and/or ice flux at the ELA. For the San Rafael and Marinelli glaciers, the average ice flux at the ELA over the past 50 years was calculated using a mass-balance budget model described in refs 11 and 45. The ice flux for Europa Glacier was reported in ref. 42, for Jorge Montt Glacier in ref. 46 and for Tyndall Glacier in ref. 47; all studies followed a similar approach to that described below.

For Fourcade Glacier of the South Shetland Islands, the cross-sectional area at the ELA (approximately 250 m above sea level) was measured using ice-penetrating radar (Extended Data Fig. 4). Velocity stakes were also installed at the ELA and tracked using a differential global positioning system (dGPS) over a two-week period in April 2007 to complement surface velocities with InSAR measurements. The use of short-term velocities measured at the end of the summer melt season produces greater uncertainties and may underestimate annual surface velocities, and hence ice flux, for this glacier system; that said, the maximum surface velocities of approximately 100 m yr^{–1} that we measured are within the range of surface velocities (60–150 m yr^{–1}) obtained from InSAR measurements averaged over 2007–2011. The potential for underestimation of the ice velocity, coupled with the predominantly volcanic bed lithology of King George Island, which suggests less resistance to mechanical and chemical erosion, may help explain (in part) why the erosion rate for Fourcade Glacier is high relative to ice motion (see Fig. 2 and Extended Data Fig. 1).

For the southernmost study glaciers of the western Antarctic Peninsula, where the ELAs are essentially at sea level, swath bathymetry was used from the ice breaker RV *Nathaniel B. Palmer* in April 2007 to determine the fjord width and depths along the ice fronts. The heights of the ice cliffs above waterline were also measured along each terminus using photogrammetry and navigational radar aboard the ice breaker RV *Nathaniel B. Palmer*. Together, the bathymetry and ice-cliff estimates were used to determine the cross-sectional area of the calving front, which represents the width-averaged ice thickness at the ELA (Extended Data Fig. 5).

To calculate the ice sliding velocity across the ELA of each glacier we followed the methods of ref. 44. The surface velocity measured from InSAR (or the velocity stakes) is the sum of the sliding and deformational velocities: $u_{\text{surface}} = u_s + u_d$.

Where some contribution of the flow is accommodated by deformation, the ice velocity decreases with depth at a rate that increases with the shear stress. We assume Glen’s flow law for the strain rate: $\dot{\epsilon} = A\tau^n$, where τ is the shear stress; with a temperature-dependent stiffness constant of $A = 1.7 \times 10^{-24} \text{ s}^{-1} \text{ Pa}^{-3}$ for subpolar ice at –2 °C for the glaciers of the Antarctic Peninsula and $A = 2.4 \times 10^{-24} \text{ s}^{-1} \text{ Pa}^{-3}$ for the temperate ice of the Patagonian glaciers; and an exponent $n = 3$.

The sliding velocity u_s is then the difference between the surface velocity u_{surface} and the depth-integrated strain rate:

$$u_s = u_{\text{surface}} - \int_0^H A(\rho g \sin(\theta))^n h^n dh$$

where

$$A(\rho g h \sin(\theta))^n = A\tau^n = \frac{du}{dh} = \dot{\epsilon}$$

is the strain rate, ρ is the density of ice, θ is the surface slope and H is the width-averaged ice thickness at the ELA. The deformation component assumes deformation by simple shear, and does not include the effect of longitudinal stress gradients or drag along valley walls. Using the known ice thickness H and the surface velocities that we measured, the maximum internal deformational velocities can be tightly constrained, and contribute no more than about 20–30 m yr^{–1} (for ice thicknesses of 400–800 m) to the total motion. Given the high surface speeds (greater than 1,000 m yr^{–1} in most cases) and modest thicknesses (a few hundred metres or less) of all of these glaciers, the ice surface velocity predominantly reflects basal sliding (93%–100% of surface speed, see Extended Data Table 1) and very little internal deformation for all glaciers in our study.

The ice discharge (flux) Q at the ELA is therefore $Q_{\text{ELA}} = Fu_s W_{\text{ELA}} H_{\text{ELA}}$, where W_{ELA} and H_{ELA} are the width and ice thickness at the ELA, respectively, and $F = (W_{\text{ELA}} + H_{\text{ELA}})/W_{\text{ELA}}$ is a semi-elliptical shape factor.

Calculating the contemporary basin-averaged bedrock erosion rate. Two cruises aboard the ice breaker RV *Nathaniel B. Palmer* during 2005 and 2007, as well as three separate cruises aboard small vessels in 2004 (Tyndall), 2006 (San Rafael) and 2010 (Jorge Montt) provided the sediment cores, acoustic reflection profiles and bathymetric data from which the sediment yields were quantified and erosion rates estimated. Cruise NBP0505 mapped the Europa and Marinelli fjords in southern Chile. Cruise NBP0703 mapped Maxwell Bay in the South Shetland

Islands, as well as six fjords along the western Antarctic Peninsula from 62° S to 65° S. Within each fjord, 3.5-kHz CHIRP and/or 100-Hz bubble pulser acoustic reflection profiles and multibeam swath bathymetry were collected (see ref. 20 for the bathymetric maps). On the basis of the detailed bathymetry and sub-bottom profiles, the sediment depocentres closest to, or abutting, the glacier termini were identified, and kasten cores were collected therein (see Extended Data Fig. 2), from which sediment accumulation rates were quantified using ^{210}Pb chronology^{20,27}.

Owing to substantial differences in accumulation rates between the fjords, we used two different methods to quantify the sediment yields from the glaciers. For temperate systems, where sediment accumulation rates close to the ice fronts of several metres per year have been observed^{11,19,20,25} and the glaciers have retreated >5 km over the last century from known terminus positions^{11,14,19,47,48,49}, the sediment yields over the past century were reconstructed from the total sediment volume mapped in the acoustic reflection profiles in the proximal fjord, within the extent of the innermost moraine, dated to >1950 AD from aerial photos^{11,48,49}. In these areas of rapid retreat and rapid sedimentation, with the exception of Europa Glacier and the distal basin of Marinelli Glacier (beyond the 1960 moraine), the short (1–2 m) kasten cores did not capture any measurable accumulation rate signal (they showed uniform, low excess ^{210}Pb in the upper 1–2 m of sediment). Hence, for these basins with rapid accumulation and a known retreat history, seismic mapping of the total sediment volume in the inner fjord provides the best measure of the modern sediment yield. When estimating yields for these glaciers, we follow the methods of refs 11, 14, 19, 48 and 49. As in similar studies, we assume that all the semi-transparent, laminated and hummocky sediment visible above a strong reflector in the sub-bottom profiles represent the post-retreat sedimentary package, deposited as the glacier terminus retreated across the fjord basin mostly in the second half of the twentieth century. Triangulated irregular network interpolation of the acoustic reflection profiles, which was used to produce gridded sediment thicknesses across the inner basins, introduces at most an 18% error in total sediment thickness, with the error increasing with both distance between profile tracks and spatial variability in the sediment thicknesses. Including a user error of 1%–2% in picking sediment depths from the seismic profiles and another 5% error in applying a median seismic velocity of $1,700\text{ m s}^{-1}$ for glaciomarine muds, we estimate that the total error in determining the sediment volume in the proximal basins from the acoustic reflection profiles is $\pm 25\%$.

In contrast, at Europa Glacier and the glaciers of the western Antarctic Peninsula, the temporal resolution of retreat and accumulation were too low to be captured in the acoustic reflection profiles. The sediment yields for Europa Glacier, the distal basin of Marinelli Glacier and the glaciers of the Antarctic Peninsula were therefore reconstructed from sediment deposition rate, on the basis of ^{210}Pb chronology in the upper 1 m of the cores²⁰; the rate was assumed to be uniform over the areal extent of the ice-proximal depocentres mapped in the swath bathymetry. ^{210}Pb chronology has been used successfully in the ice-distal regions of temperate fjords^{19,20,49,50} and throughout polar fjords^{12,20,27}; it provides the sediment accumulation rate in each depocentre averaged over the past century (about five ^{210}Pb half-lives). In a few fjords (Cierva Cove and Collins Bay), the profiles show little or no excess ^{210}Pb , suggesting either no substantial accumulation (which goes against all circumstantial evidence, including a thick drape of soft, unconsolidated sediments) or (which is more likely) a rapid accumulation of >1 m of sediment that did not sequester appreciable ^{210}Pb from the fjord water column²⁰. For these glaciers, it was not possible to derive erosion rates. From the acoustic reflection profiles (archived in ref. 51), it was clear that in most instances: (1) the sediment layers were of uniform thickness across each depocentre, which leads us to assume that once the sediment has been diffusively redistributed along the bottom of the fjord, accumulation is spatially uniform across each depocentre, despite the large variation in deposition rates observed in temperate fjords^{19,20,49,50}; and (2) the bedrock highs surrounding these depocentres were devoid of a sediment drape, and hence we assume that all the sediment delivered by the glacier collected in the basin lows, whether by direct rain-out of fine sediment from the water column or through gravitational redistribution of sediment that had collected on the steep flanks of the fjord and sills. We recognize that in all cases these depocentres are not entirely closed systems, and that there is potential for some of the sediment to by-pass the most proximal depocentre through entrainment in the water column, or to 'leak' from the depocentre through resuspension and remobilization downfjord. If a substantial portion of the sediment is transported beyond the fjord, our estimates of sediment yield within the proximal depocentres would not capture the total volume of sediment being eroded and delivered by the glacier. To address this, in four of the fjords (Marion Cove (Maxwell Bay), Andvord Bay, Flandres Bay and Beascochea Bay) sediment cores were also collected in the middle/outer fjord depocentres, from which modern accumulation rates were also estimated using ^{210}Pb and ^{137}Cs chronologies²⁷. From these outer basins, we

estimate that 46%–54% of the total sediment flux from the glaciers are by-passing the proximal depocentre. Hence, the sediment yields we are measuring from the proximal basins represent approximately half of the total flux; we assumed this to be true for all fjords that do not have prominent outer sills, we doubled the estimated sediment yields that are based on only the proximal basins.

The varying distribution of accumulation within each fjord and the percentage of sediment lost beyond the proximal basins, present a distinct challenge for estimating basin-averaged erosion rates in 'open' fjord systems. In addition, we recognize the limitations of using one or two point measurements of sediment accumulation rates from each basin to calculate total sediment yields. The sediment cores in the most proximal basin were generally collected more than 500 m from the ice front (with the exception of Trooz Glacier, see ref. 20), and probably do not capture the highest accumulation rates that are expected close to the ice front. Thus, our assumption that the measured sediment accumulation rates^{20,27} are representative of the entire proximal basin depocentre probably also underestimates the total volume of sediment delivered by the glacier, and thus the erosion rate. We also assume that the contribution of non-terrestrial, biogenic material to the fjord sediment is small, less than 10% of the overall sediment volume deposited^{20,27}.

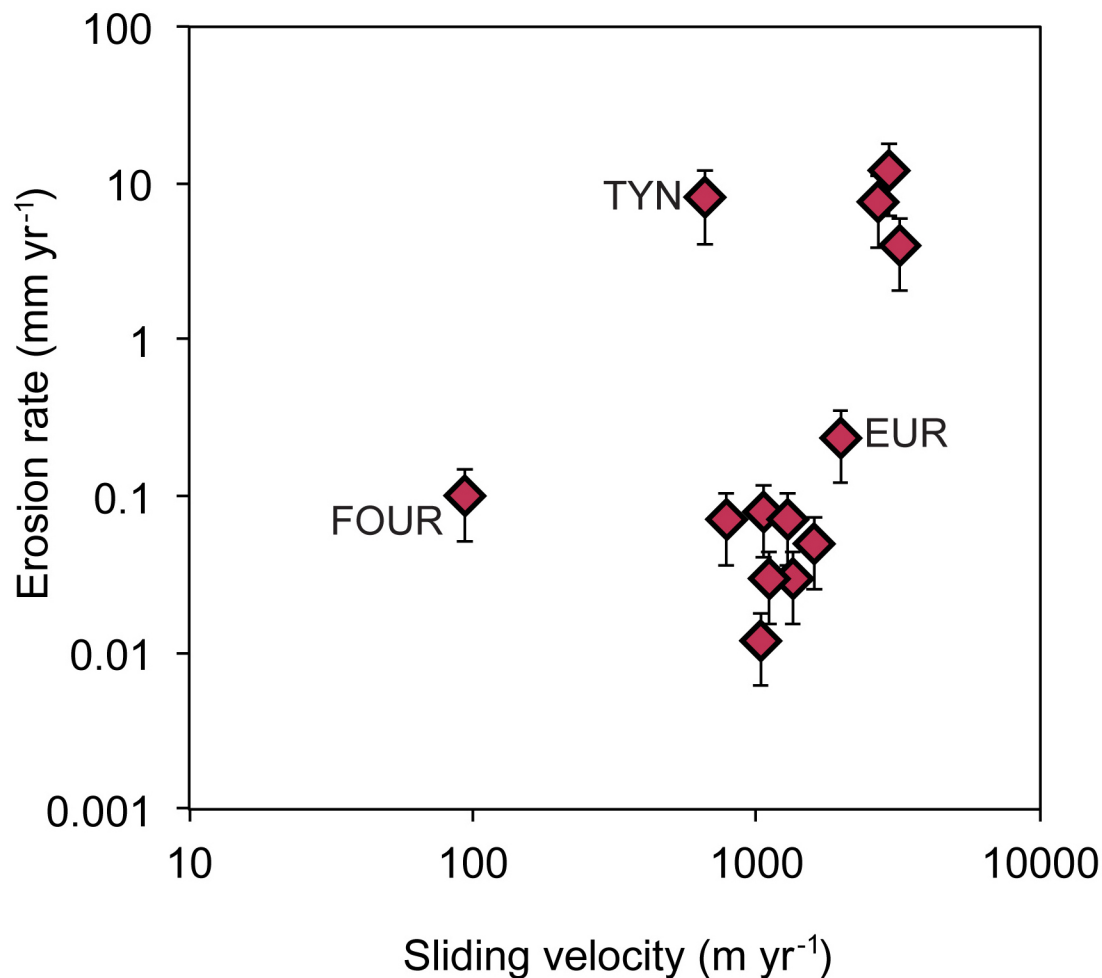
At Marinelli Glacier, the accumulation rates in the distal basin were small enough that we were able to compare the sediment yields calculated using the total sediment volume from the proximal basin with those using ^{210}Pb chronology from a core in the distal depocentre (12 km from the current terminus, and outside of a moraine that the glacier retreated from around 1960^{11,14,20}); see Extended Data Fig. 6. For this glacier system, the ^{210}Pb measurement of distal accumulation produced sediment yields that were about a third (36%) of the yield that was estimated from the total sediment volume in the proximal basin (see Extended Data Table 1). However, in this instance, comparison of the two methods is complicated by real differences in local and basin-wide measurements and in proximity to the ice front, and hence proximity to the highest rates of accumulation, over the centennial timescale of measurement. Nevertheless, the comparison of the two methods to measure sediment yields at this one location suggests that any methodological biases produce a factor of 2–3 difference in estimates at most, but clearly cannot account for the differences of over two orders of magnitude in the sediment yields, and by inference erosion rates, between temperate and polar systems.

Using both measurement approaches, the 100-year-averaged sediment yield (in cubic metres per year) is then converted to a basin-wide sediment production rate per unit area by dividing the yield by the glacier catchment area, measured from 2005 Landsat imagery, the 2000 Shuttle Radar Topography Mission digital elevation model (SRTM DEM; for Patagonia) and the British Antarctic Survey's Radarsat 200-m digital elevation model (for the Antarctic Peninsula); see Extended Data Fig. 2. To convert the sediment production rate to a bedrock erosion rate, the former is multiplied by the ratio between the dry bulk density of glaciomarine sediment ($1,300\text{ kg m}^{-3}$, the median density measured from the sediment cores) and that of crystalline metasedimentary and igneous bedrock (approximately $2,700\text{ kg m}^{-3}$). Using this approach, we derive a centennially averaged, basin-averaged bedrock erosion rate for each glacier catchment. The range of bedrock and sediment densities introduces an additional uncertainty in the calculation of the bedrock erosion rate of up to 12%. Hence, combined with uncertainties in our assumption of the terrestrial origin of all sediment, not accounting for spatial variations in the sediment accumulation rate and in the areal extent of deposition, the cumulative known uncertainty in our calculated basin-wide erosion rates approaches 38% for the temperate fjords and 50% for Europa and the polar fjords, and all are probably underestimates of the total erosion and sediment produced by the glaciers.

The relationship between erosion and sliding. To compare our findings regarding the relationship between erosion and sliding (the 'erosion rule') to what has been used in numerical models (Fig. 2d), we employed a nonlinear least-squares regression analysis using the 'nls' package in R⁵² to estimate the two constants of proportionality, K_g and n , from the erosion rule $E = K_g u_s^n$, where u_s and E are our observations of basal sliding speed and estimates of erosion rate for each glacier, respectively. We computed the mean and standard deviation of the erosion rates and ice velocities. We then ran the nonlinear least-squares model within the 95% confidence interval of the observed data, assuming both the power-law distribution, and an exponential distribution of the form $E = \alpha e^{bu_s}$. We also used a linear least-squares fit for comparison. The best-fit model (residual standard error, $\text{RSE} = 0.00335$; residual sum-of-squares error, $\text{RSS} = 0.0001246$; $r^2 = 0.39$) using the nonlinear least-squares method for all glaciers in the data set ($n = 13$) returned a power-law distribution with coefficients $K_g = 5.2 \times 10^{-8}$ and $n = 2.34$. Using the same suite of nonlinear models and excluding the two outlier data—Tyndall Glacier and Fourcade Glacier (see

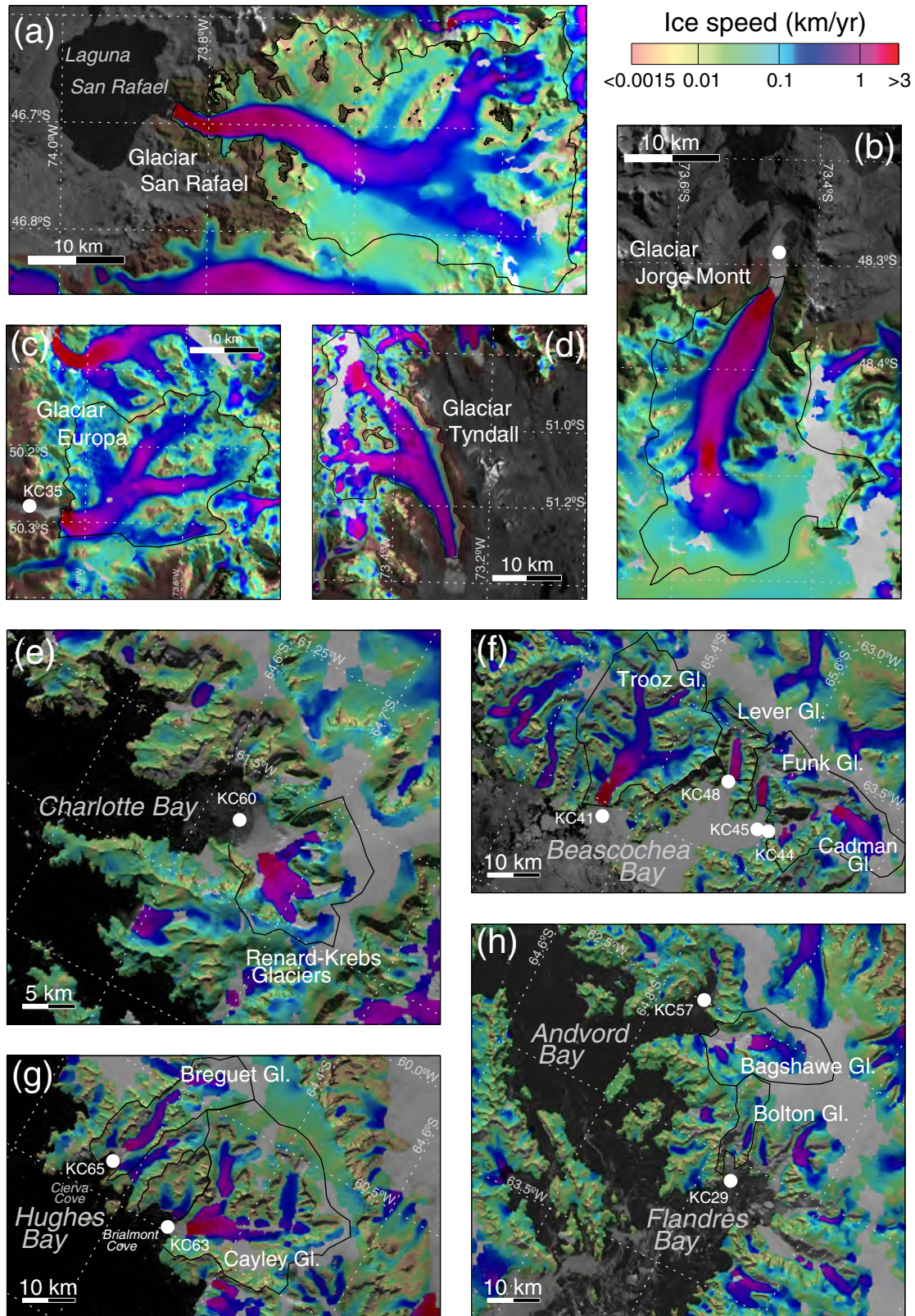
Extended Data Fig. 1)—also resulted in a best-fit power-law distribution ($r^2 = 0.62$) with coefficients $K_g = 5.3 \times 10^{-9}$ and $n = 2.62$.

33. Dalziel, I. W. D. *et al.* The Scotia arc: genesis, evolution, global significance. *Annu. Rev. Earth Planet. Sci.* **41**, 767–793 (2013).
34. Breitsprecher, K. & Thorkelson, D. J. Neogene kinematic history of Nazca–Antarctic–Phoenix slab windows beneath Patagonia and the Antarctic Peninsula. *Tectonophysics* **464**, 10–20 (2009).
35. Guillaume, B. *et al.* Dynamic topography control on Patagonian relief evolution as inferred from low temperature thermochronology. *Earth Planet. Sci. Lett.* **364**, 157–167 (2013).
36. Mayr, C. *et al.* Holocene variability of the Southern Hemisphere westerlies in Argentinean Patagonia (52° S). *Quat. Sci. Rev.* **26**, 579–584 (2007).
37. Vaughan, D. G. *et al.* Recent rapid regional climate warming on the Antarctic Peninsula. *Clim. Change* **60**, 243–274 (2003).
38. Turner, J. *et al.* Antarctic climate change during the last 50 years. *Int. J. Climatol.* **25**, 279–294 (2005).
39. Cook, A. J., Fox, A. J., Vaughn, D. G. & Ferrigno, J. G. Retreating glacier fronts on the Antarctic Peninsula over the past half-century. *Science* **308**, 541–544 (2005).
40. Cook, A. J., Vaughn, D. G., Luckman, A. & Murray, T. A new Antarctic Peninsula glacier basin inventory and observed area changes since the 1940s. *Antarct. Sci.* **26**, 614–624 (2014).
41. Pritchard, H. D. & Vaughn, D. G. Widespread acceleration of tidewater glaciers on the Antarctic Peninsula. *J. Geophys. Res.* **112**, F03S29 (2007).
42. Forster, R. R., Rignot, E., Isacks, B. L. & Jezek, K. C. Interferometric observations of Glaciares Europa and Penguin, Hielo Patagonico Sur, Chile. *J. Glaciol.* **45**, 325–337 (1999).
43. Mougint, J. & Rignot, E. Ice motion of the Patagonian Icefields of South America: 1984–2014. *Geophys. Res. Lett.* **42**, 1441–1449 (2015).
44. Rignot, E., Mougint, J. & Scheuchl, B. Ice flow of the Antarctic Ice Sheet. *Science* **333**, 1427–1430 (2011).
45. Koppes, M., Conway, H., Rasmussen, L. A. & Chernos, M. Deriving mass balance and calving variations from reanalysis data and sparse observations, Glaciar San Rafael, northern Patagonia, 1950–2005. *Cryosphere* **5**, 791–808 (2011).
46. Rivera, A., Corripio, J., Bravo, C. & Cisternas, S. Glaciar Jorge Montt (Chilean Patagonia) dynamics derived from photos obtained by fixed cameras and satellite image feature tracking. *Ann. Glaciol.* **53**, 147–155 (2012).
47. Raymond, C. *et al.* Retreat of Glaciar Tyndall, Patagonia, over the last half-century. *J. Glaciol.* **51**, 239–247 (2005).
48. Koppes, M., Sylwester, R., Rivera, A. & Hallet, B. Variations in sediment yield over the advance and retreat of a calving glacier, Laguna San Rafael, North Patagonian Icefield. *Quat. Res.* **73**, 84–95 (2010).
49. Boldt, K. V. *Fjord sedimentation during the rapid retreat of tidewater glaciers: observations and modeling*. PhD thesis, Univ. Washington (2014).
50. Jaeger, J. M., Nittouer, C. A., Scott, N. D. & Milliman, J. D. Sediment accumulation along a glacially impacted mountainous coastline: north-east Gulf of Alaska. *Basin Res.* **10**, 155–173 (1998).
51. Carbotte, S. M. *et al.* *Antarctic Multibeam Bathymetry and Geophysical Data Synthesis: an on-line digital data resource for marine geoscience research in the Southern Ocean*. Open-file Report No. 2007-1047-SRP-002 (US Geological Survey, 2007).
52. Baty, F. *et al.* A toolbox for nonlinear regression in R: the package nlstools. *J. Stat. Softw.* **66**, 5 (2015).



Extended Data Figure 1 | Erosion rate versus sliding velocity for 13 outlet glaciers. A log-log plot, showing a general power-law relationship between erosion and basal ice motion, and two outliers: Fourcade Glacier (FOUR) and Tyndall Glacier (TYN). The nonlinear least-squares best-fit estimate using all

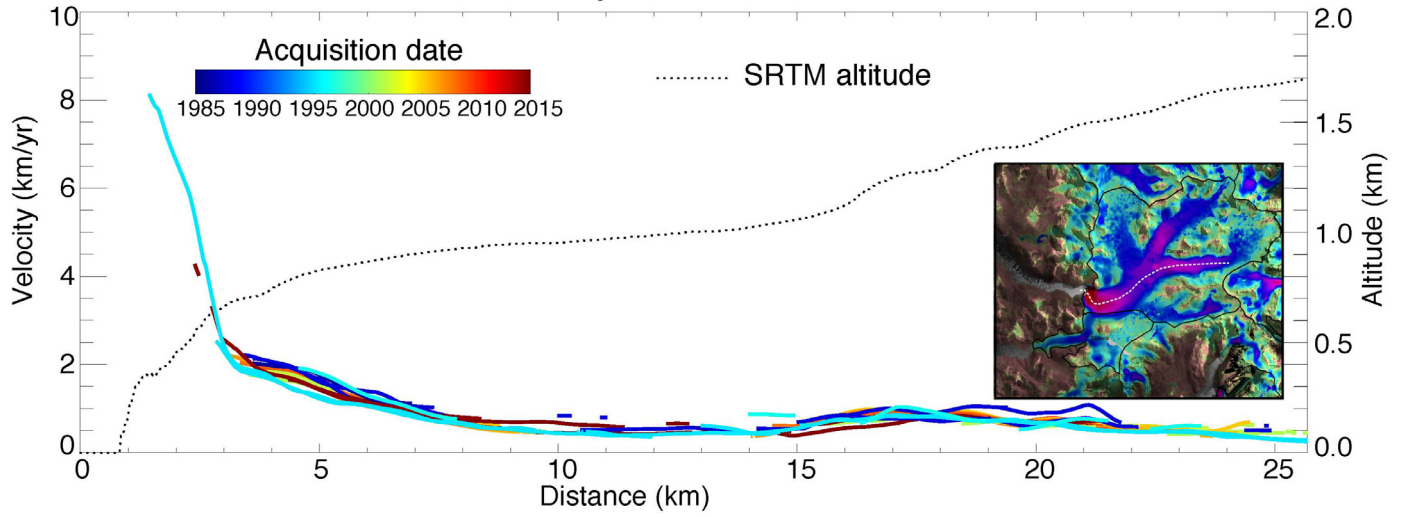
glaciers yields an exponent $n = 2.34$ and intercept $K_g = 5.2 \times 10^{-8}$ ($r^2 = 0.39$); excluding the two outliers, the fit improves, with $n = 2.62$ and intercept $K_g = 5.3 \times 10^{-9}$ ($r^2 = 0.62$).



Extended Data Figure 2 | Ice motion for outlet glaciers of Patagonia and western Antarctic Peninsula. a–h, Glacier catchment areas (within the black outline) with InSAR-derived ice velocities (in km yr^{-1}) from 2007–2008 superimposed (indicated by the colour scale). The InSAR velocity maps are modified from data from refs 43 and 44. White dots indicate the location of

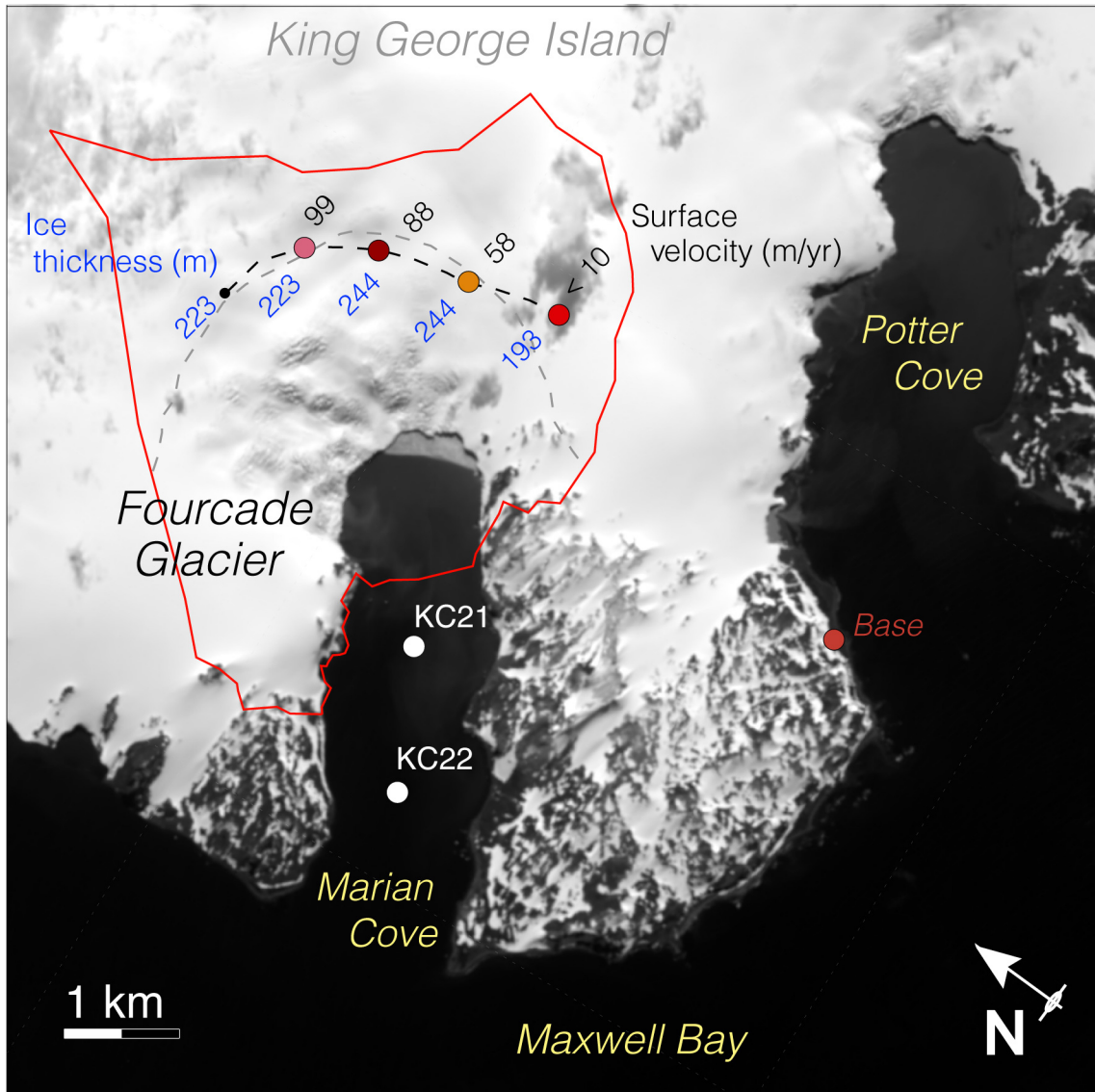
the cores in ice-proximal depocentres from which accumulation rates were measured (see refs 20, 27 and 49). Catchment areas shown are San Rafael (a), Jorge Montt (b), Europa (c), Tyndall (d), Charlotte Bay (e), Beascochea Bay (f), Hughes Bay (g), and Andvord and Flandres Bays (h).

Europa Glacier



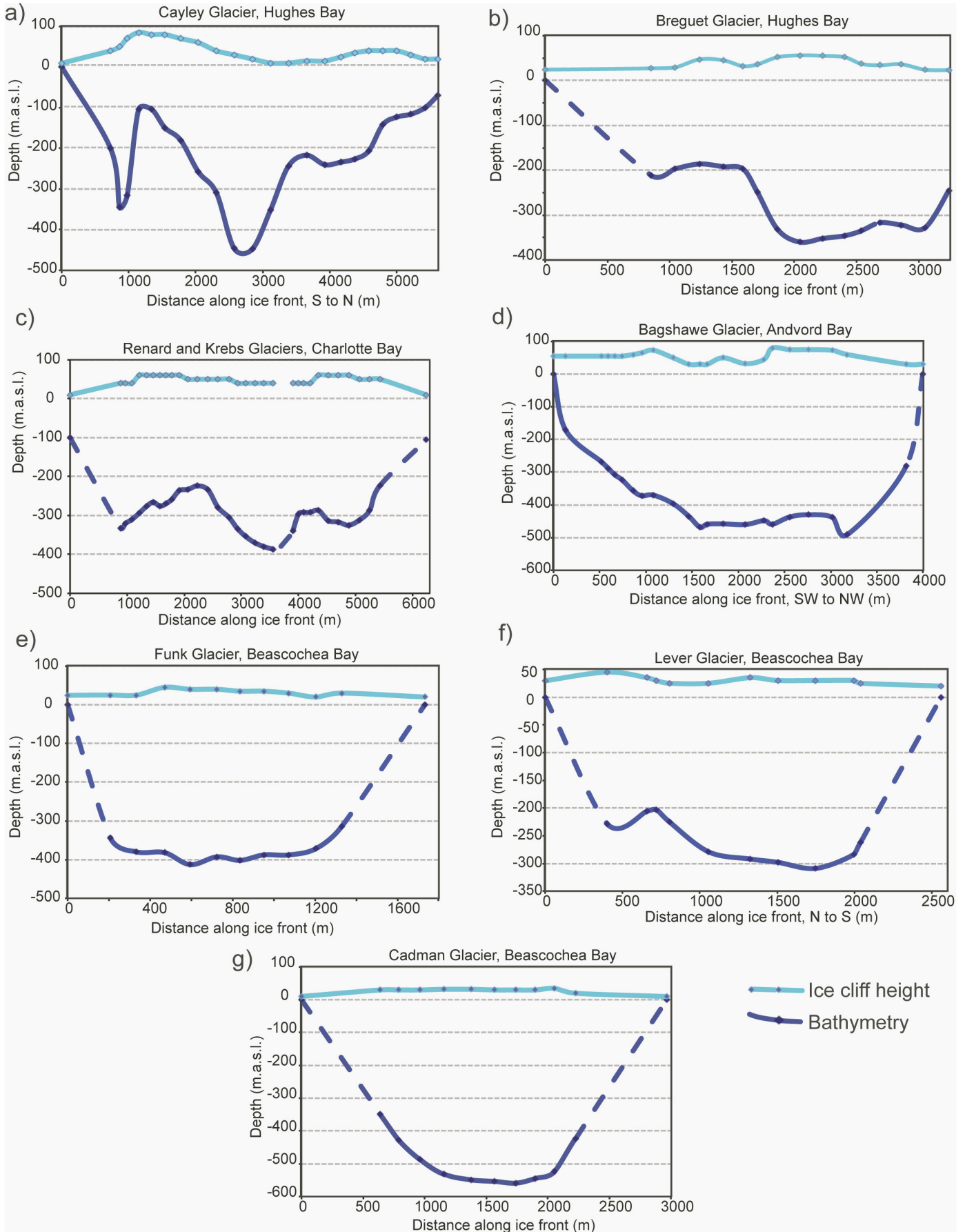
Extended Data Figure 3 | Surface elevation and time series of surface velocity along the central flowline for Europa Glacier, South Patagonian Icefield. The black dashed line is the elevation profile from the terminus, derived from the 2001 SRTM DEM. Flow speeds were measured along the

centreline from InSAR repeat image pairs (see ref. 43), coloured according to the year the data were acquired. Inset is Extended Data Fig. 2c, with the overlaid white dashed line indicating the centreline of the glacier.



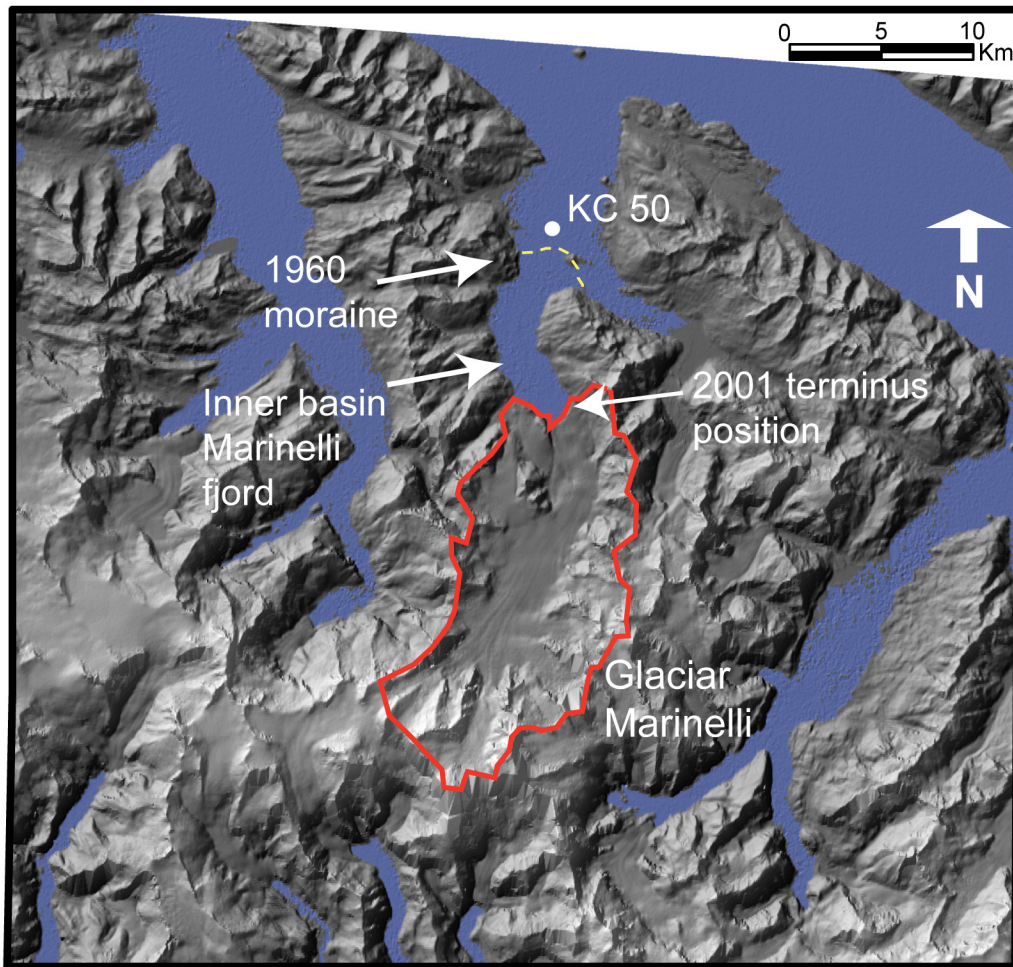
Extended Data Figure 4 | Ice thickness and surface velocity across Fourcade Glacier, King George Island. The red line indicated the glacier catchment area in 2007; the black dashed line shows the path of the ice-penetrating radar; and the grey dashed line is the ELA (approximately 250 m above sea level).

Surface velocities from dGPS of velocity stakes (April 2007) are in black and ice thickness measurements from ice-penetrating radar are in blue. Base indicates location of dGPS base station.



Extended Data Figure 5 | Ice-front cross-sectional areas of the polar glaciers of the western Antarctic Peninsula. a–g, The light blue lines are the ice cliff heights above the water line and the dark blue lines are the submarine ice faces from the swath bathymetry; m.a.s.l., metres above sea level. Dashed lines indicate interpolated ice thicknesses between known points. For all

glaciers, the ELA is located at the calving front. Measurements are for Cayley Glacier, Hughes Bay (a), Breguet Glacier, Hughes Bay (b), Renard and Krebs glaciers, Charlotte Bay (c), Bagshawe Glacier, Andvord Bay (d), Funk Glacier, Beascochea Bay (e), Lever Glacier, Beascochea Bay (f) and Cadman Glacier, Beascochea Bay (g).



Extended Data Figure 6 | Glacier and fjord catchment area for Marinelli Glacier, Cordillera Darwin Icefield. The glacier catchment area in 2009 is indicated by the red line; the location of Little Ice Age moraine from which the glacier terminus retreated around 1960 is indicated by the yellow dashed line; the inner basin of the fjord where acoustic reflection profiles

captured total sediment volume since 1960 is indicated by the appropriate arrow (see ref. 11); and the white dot indicates the location of the sediment core in the distal depocentre from which the distal accumulation rate was measured (see ref. 20).

Extended Data Table 1 | Glacier characteristics and corresponding erosion rates in Chilean Patagonia and the Antarctic Peninsula.

GLACIER	Location	Lat.	Long.	Cross-sectional area		Width of calving front ²	MAX surface velocity ³	Ratio basal: surface velocity ⁴	ICE FLUX ⁵	dx/dt ⁴	Sediment Accumulation Rate ⁵	Proximal depocentre area ⁶	Erosion Rate ^{7,8}
				Catchment Area ¹	front ²								
<i>Patagonia</i>													
San Rafael (SR)	NPI	46.66	73.82	728	0.42	2.2	>2800	100	0.75-2.3	-88	643	13.9	12 ± 4
Jorge Montt (JM)	SPI	48.3	73.5	500	0.44	1.6	>3600	100	2.1	-278	>400	4	4 ± 1.2
Europa (EUR)	SPI	50.28	73.92	409	0.27	1.1	1970	100	0.54		11.4	8.98	0.24 ± 0.12
Tyndall (TYN)	SPI	51.25	73.27	418	0.44	1.9	700	100	0.83	-123		1.8	8 ± 2.4
Marinelli (MAR)	CDI	54.39	69.59	154	0.23	1.8	>1000	100	0.5-1.17	-289	>500	21.7	7.6 ± 2.3
											23.6	42	2.71 ± 1.3
<i>S. Shetland Is.</i>													
Fourcade (FOUR)	Marion Cove	62.21	58.75	241	0.90	4.1	100	96	0.09	-6.86	6.6, 2.8	0.26, 0.29	0.10 ± 0.05
<i>Antarctica Pen.</i>													
Breguet	Cierva Cove	64.16	60.85	261	0.74	3.5	880	96	1.64	-4.9	uniform	1.1	n/a
Cayley (CAY)	Brailmont Cove	64.30	60.98	720	1.44	5.6	1670	97	2.48	-1.7	15	2.47	0.05 ± 0.03
Renard-Krebs (RK)	Charlotte Bay	64.66	61.62	118	0.95	4.3	1200	95	0.5	-4.9	2.8	1.51	0.03 ± 0.02
Bagshawe (BAG)	Andvord Bay	64.91	62.61	241	1.66	5.8	1450	93	0.76	7.7	5.6	2.06	0.07 ± 0.03
Bolton (BOL)	Flandres Bay	65.07	62.97	62	0.62	2.6	1100	98	1.01	-55	2.8	3.77	0.08 ± 0.04
Trooz	Collins Bay	65.33	63.97	633	0.94	3.3	>1360	98	1.57	37.6	uniform	2.26	n/a
Lever (LEV)	Beascochea Bay	65.51	63.69	177	1.20	2.6	>800	98	0.65	-4.2	6.4	2.23	0.07 ± 0.03
Funk (FUN)	Beascochea Bay	65.58	63.78	142	0.58	1.7	1075	97	0.69	-4.1	2.0	2.47	0.01 ± 0.005
Cadman (CAD)	Beascochea Bay	65.61	63.82	306	1.15	3.0	>1500	93	2.23	16.3	7.0	1.65	0.03 ± 0.02

CDI, Cordillera Darwin Icefield; NPI, North Patagonian Icefield; SPI, South Patagonian Icefield.

¹ Glacier basin area was measured from 2005 Landsat 7, 2013 Landsat Enhanced Thematic Mapper imagery and the British Antarctic Survey's Radarsat 200-m DEM (see Extended Data Fig. 2).

² Width of calving-front and ice-front cross-sectional area was measured from swath bathymetry and ice cliff height (see Extended Data Fig. 5).

³ Maximum and width-averaged surface ice flow speed at ELA was measured from InSAR velocity map (see Extended Data Fig. 2).

⁴ Retreat rates (dx/dt) for individual glaciers in the latter half of the twentieth century were reported in ref. 39.

⁵ Sediment accumulation rates were calculated from ²¹⁰Pb decay profiles in top 1 m of cores, reported in refs 20 and 27. Accumulation rates, and therefore erosion rates, from vertically uniform ²¹⁰Pb profiles could not be determined.

⁶ Depocentre basin area was measured from multibeam swath bathymetry and 3.5-kHz sub-bottom acoustic reflection profiles (see ref. 20 for bathymetric maps and data repository in ref. 51 for acoustic profiles).

⁷ Bedrock erosion rate was calculated by dividing the centennial sediment yield (the product of sediment accumulation rate and depocentre area) by the glacier catchment area, taking into account the dry bulk densities of glacial marine sediment (on average, 1.3 g cm⁻³) and crystalline bedrock (on average, 2.7 g cm⁻³). Erosion rates for San Rafael, Jorge Montt, Tyndall and Marinelli glaciers (inner basin) were calculated using the total sediment volume deposited since 1960 in the basin closest to the ice front, measured from acoustic reflection profiles and repeat bathymetry (see refs 11, 48, and 49).

⁸ Estimates of centennial sediment yield for the Antarctic Peninsula and Europa glaciers were doubled from the yields measured in the proximal depocentre to account for downfjord losses in accumulation, as estimated from accumulation rates in the middle and outer basins of Marion Cove (Maxwell Bay), Andvord Bay (ref. 27), Flandres Bay and Beascochea Bay.